European Radiology (2023) 33:8122–8131
https://doi.org/10.1007/s00330-023-09805-8

European Radiology
EUROPEAN SOCIETY OF RADIOLOGY

BREAST

Ultrafast DCE-MRI for discriminating pregnancy-associated breast cancer lesions from lactation related background parenchymal enhancement

Noam Nissan[1,2] · Debbie Anaby[1,2] · Gazal Mahameed[1,2] · Ethan Bauer[2] · Efi Efraim Moss Massasa[1] · Tehillah Menes[3] · Ravit Agassi[4] · Asia Brodsky[5] · Robert Grimm[6] · Marcel Dominik Nickel[6] · Elisa Roccia[7] · Miri Sklair-Levy[1,2]

Received: 22 September 2022 / Revised: 31 March 2023 / Accepted: 27 April 2023 / Published online: 6 June 2023

Abstract

Objective To investigate the utility of ultrafast dynamic-contrast-enhanced (DCE) MRI in visualization and quantitative characterization of pregnancy-associated breast cancer (PABC) and its differentiation from background-parenchymal-enhancement (BPE) among lactating patients.

Materials and methods Twenty-nine lactating participants, including 10 PABC patients and 19 healthy controls, were scanned on 3-T MRI using a conventional DCE protocol interleaved with a golden-angle radial sparse parallel (GRASP) ultrafast sequence for the initial phase. The timing of the visualization of PABC lesions was compared to lactational BPE. Contrast-noise ratio (CNR) was compared between the ultrafast and conventional DCE sequences. The differences in each group's ultrafast-derived kinetic parameters including maximal slope (MS), time to enhancement (TTE), and area under the curve (AUC) were statistically examined using the Mann–Whitney test and receiver operator characteristic (ROC) curve analysis.

Results On ultrafast MRI, breast cancer lesions enhanced earlier than BPE ($p < 0.0001$), enabling breast cancer visualization freed from lactation BPE. A higher CNR was found for ultrafast acquisitions vs. conventional DCE ($p < 0.05$). Significant differences in AUC, MS, and TTE values were found between the tumor and BPE ($p < 0.05$), with ROC-derived AUC of 0.86 ± 0.06, 0.82 ± 0.07, and 0.68 ± 0.08, respectively. The BPE grades of the lactating PABC patients were reduced as compared with the healthy lactating controls ($p < 0.005$).

Conclusion Ultrafast DCE MRI allows BPE-free visualization of lesions, improved tumor conspicuity, and kinetic quantification of breast cancer during lactation. Implementation of this method may assist in the utilization of breast MRI for lactating patients.

Clinical relevance The ultrafast sequence appears to be superior to conventional DCE MRI in the challenging evaluation of the lactating breast. Thus, supporting its possible utilization in the setting of high-risk screening during lactation and the diagnostic workup of PABC.

Key Points

- *Differences in the enhancement slope of cancer relative to BPE allowed the optimal visualization of PABC lesions on mid-acquisitions of ultrafast DCE, in which the tumor enhanced prior to the background parenchyma.*
- *The conspicuity of PABC lesions on top of the lactation-related BPE was increased using an ultrafast sequence as compared with conventional DCE MRI.*
- *Ultrafast-derived maps provided further characterization and parametric contrast between PABC lesions and lactation-related BPE.*

✉ Noam Nissan
noamniss@gmail.com

[1] Department of Radiology, Sheba Medical Center, Emek Ha-Ella 1 St. Tel Hashomer, 5265601 Ramat Gan, Israel

[2] Sackler School of Medicine, Tel Aviv University, Tel Aviv, Israel

[3] Department of General Surgery, Sheba Medical Center, Ramat Gan, Israel

[4] Department of General Surgery, Soroka Medical Center, Beersheba, Israel

[5] Department of General Surgery, Bnei Zion Medical Center, Haifa, Israel

[6] MR Application Predevelopment, Siemens Healthcare GmbH, Erlangen, Germany

[7] MR Scientific Marketing, Siemens Healthcare GmbH, Erlangen, Germany

Keywords Breast neoplasms · Magnetic resonance imaging · Lactation · Ultrafast · Pregnancy-associated breast cancer

Abbreviations

AUC	Area under the curve
BPE	Background parenchymal enhancement
BPU	Background parenchymal uptake
CAD	Computer-aided diagnosis
CNR	Contrast-noise ratio
DWI	Diffusion-weighted imaging
DCE	Dynamic contrast enhanced
TE	Echo time
FOV	Field of view
FDG	Fluorodeoxyglucose
GRASP	Golden-angle radial sparse parallel
IDC	Invasive ductal carcinoma
CNRmax	Maximal BPE contrast noise ratio
ROImax	Maximal BPE regions of interest
MS	Maximum slope
CNRnormal	Normal BPE contrast noise ratio
ROInormal	Normal BPE regions of interest
PACS	Picture archiving and communication system
PABC	Pregnancy-associated breast cancer
ROC	Receiver operating characteristic
ROI	Regions of interest
TR	Repetition time
SI	Signal intensity
SPAIR	Spectral attenuated inversion recovery
SD	Standard deviations
TTE	Time to enhancement
TWIST	Time-resolved angiography with a stochastic trajectory

Introduction

The lactating breast is characterized by unique physiological and morphological characteristics, which generate a diagnostic challenge from both clinical and radiological perspectives [1]. At the beginning of pregnancy, the mammary gland increases substantially in size and develops a greater proportion of glandular tissue. This increases the mammographic density of the breast, which in turn, reduces the sensitivity of mammography in the detection of lesions [2]. In addition, as a result of the increased metabolic demand of breastfeeding, the lactating breast develops an abundant vascular network [3], which typically presents as a marked background parenchymal enhancement (BPE) on dynamic contrast-enhanced (DCE) MRI [4].

Pregnancy-associated breast cancer (PABC) is defined as breast cancer diagnosed during pregnancy, in the first postpartum year, or at any time during lactation. The diagnosis of PABC is often delayed, and therefore, it is associated with a poor prognosis [5]. In the wake of the marked BPE associated with lactation, the utilization of breast MRI has been debated [6–8]. Several preliminary MRI studies have suggested that PABC lesions could be detected despite the marked BPE [9–14], including a recent study that reported 93% sensitivity of breast MRI during lactation [14]. Lactation-related BPE has been found to reduce tumor conspicuity by up to 60% [13] and is further associated with false-positive flagging by computer-aided diagnosis (CAD) [15].

In recent years, the emergence of compressed sensing MRI has prompted the development of new accelerated pulse sequences [16]. Implementation of sparse techniques for breast MRI has led to the introduction of ultrafast DCE [17, 18]. This approach has improved the temporal resolution by a factor of ten, allowing the acquisition of sequential fast DCE images in the first-minute post-contrast and the quantification of the wash-in kinetics. Initial breast ultrafast MRI studies have reported promising results in discriminating benign from malignant breast lesions, prognostication of breast cancer, and monitoring response to chemotherapy [19–31].

Breast cancer tends to exhibit a fast wash-in slope on the initial ultrafast acquisitions and BPE usually demonstrates a slow early enhancement slope, followed by a persistent delayed enhancement [32]. Considering these features, we hypothesize that the ultrafast sequence might therefore be particularly suitable for the challenges posed by the lactating breast and improve the contrast between PABC and lactation-related BPE. In this study, our initial experience with ultrafast MRI of lactating patients is presented, focusing on the visualization of PABC and lactation-related BPE compared with a conventional DCE sequence, as well as on their quantitative characterization via ultrafast-derived kinetic parametric mapping.

Materials and methods

Patients

The study was approved by our institutional Internal Review Board and the necessity to acquire a signed informed consent was waived due to the retrospective nature of the study. The study population was comprised of 29 lactating examinees, including 10 PABC patients (median age: 35 years, range: 27–42) and 19 healthy lactating controls (median age: 37 years, range: 28–42), whose MRI was clinically indicated regardless of the study. All scans were performed between August 2021 and June 2022 using our newly-adopted clinical protocol with an embedded ultrafast sequence. All PABC patients had newly diagnosed, biopsy-confirmed breast cancer and were scanned for pre-treatment evaluation. PABCs

included invasive ductal carcinoma (IDC) (mean lesion size of 3.4 ± 2.2 cm, range: 0.7–7.5 cm). All controls were BRCA carriers scanned for annual high-risk surveillance.

MRI technique

All scans were performed on a 3-T MRI scanner (MAGNETOM Vida; Siemens Healthcare) with a dedicated 16-channel bilateral breast coil. The MRI protocol included a Dixon T2-weighted acquisition followed by two dynamic series. This included a conventional high-resolution T1-weighted before and four times after contrast administration, interleaved with a series of 11 ultrafast acquisitions acquired continuously during the first minute of contrast media inflow. Automatic injection of contrast agent bolus (0.1 mL/kg at 2 mL/s Dotarem (gadoterate meglumine)) was used followed by a 20-mL saline flush. The ultrafast protocol was based on the golden-angle radial sparse parallel (GRASP) technique [33, 34] with a compressed sensing reconstruction, using the following parameters: Repetition time/ echo time (TR/TE) = 3.6/1.55 ms, flip angle = 12°, bandwidth = 590 Hz, field of view (FOV) = 340 mm and matrix = 256 × 256, yielding a spatial resolution of 1.3 × 1.3 mm and 144 slices of 1.5 mm thickness. The temporal resolution was 6.1 s per acquisition and the total acquisition time was 71 s. The conventional dynamic series were based on spectral attenuated inversion recovery (SPAIR) and acquired with the following parameters: TR/TE = 5/1.38 ms, flip angle = 10°, bandwidth = 770 Hz, matrix = 352 × 316 and FOV = 360 mm yielding a spatial resolution of 1 × 1 mm and 144 slices of 1.5 mm. The total acquisition time was 4:30 min, which is almost equivalent to the standard clinical protocol for breast MRI [26].

Image analysis

Two reporting radiologists, N.N. and M.S.L., with 11 and 24 years of experience in breast MRI read the scans by consensus. Regions of interest (ROIs) of the tumor were manually delineated on three central axial slices to measure the signal intensity (SI) at each time point, excluding the clip marker and apparent necrotic tissue, using commercial PACS (picture archiving and communication system) workstation. The earliest time point at which the tumor was visualized was determined objectively based on the scan in which the increment in SI in the tumor's ROI exceeded a 30% increase compared with the pre-injection T1-weighted image. This threshold was fixed in accordance with the previous report which stated that it provided the highest sensitivity and correlation with pathological tumor size [35]. In addition to the tumor's ROI, due to the heterogeneous BPE distribution, two reference ROIs of the healthy contralateral fibroglandular tissue were measured: ROI_{Normal}, presented in the reciprocal area of the same slice of the contralateral breast and ROI_{Max}, delineated in the contralateral breast, not necessarily in the same slice, but where the BPE appeared most marked. Tumor conspicuity was determined using contrast-noise ratio (CNR) analysis [36], using two sets of CNR measures: CNR_{Normal} and CNR_{Max}, respectively. Finally, using prototype software (MR DCE; Siemens Healthcare), the GRASP datasets were processed to derive color-coded parametric maps time to enhancement (TTE), maximum slope (MS), and the area under the relative enhancement curve (AUC) for the initial 60 s after enhancement onset [19]. A summary of the analysis type for each group of patients is given in Table 1.

Statistical analysis

The first volume of the ultrafast acquisition, in which the tumor and BPE_{Max} exceeded the threshold of 30%, was determined for each patient individually and compared using a paired two-way Student's t-test. For each patient, the highest CNR in each sequence served as the comparison for tumor conspicuity between ultrafast and conventional DCE sequences. For CNR analysis, the mean and standard deviation (SD) values were measured for each temporal DCE time point, yielding sequential column plots (GraphPad Prism 5.03). The Mann–Whitney test was applied for evaluating differences in BPE grades (recorded in the original MRI report) between groups of healthy lactating and PABC patients. Additionally, this test was also used for evaluating differences between ultrafast-derived parameters among PABC and healthy lactating controls for the two ROIs. The Wilcoxon test was applied for evaluating intra—individual differences between ultrafast-derived parameters of PABC patients. The receiver operating characteristic (ROC) curve was used to test the utility of the ultrafast kinetic parameters to differentiate between tumor

Table 1 Analysis type per group and number of patients

Group	Number of patients	Analysis
PABC	$n = 10$	Time to visualization and CNR
PABC	$n = 10$	Quantitative ultrafast kinetic parameters in tumor and BPE (TTE, MS, AUC)
PABC vs. controls	$n = 29$	Quantitative BPE ultrafast kinetic parameters (TTE, MS, AUC) and grades in PABC patients vs. lactating controls

and BPE measurements. Statistical analysis was performed using R (R Core Team. R: A language and environment for statistical computing. R Foundation for Statistical Computing, 2020). Statistical significance was defined as $p < 0.05$.

Results

Visualization of breast cancer and lactation BPE using ultrafast DCE

Inspection of the SI kinetics of the tumor and lactating parenchyma showed that PABC lesions enhanced at least one acquisition prior to the presence of BPE ($p < 0.0001$), enabling breast cancer visualization freed from lactation BPE. The typical SI buildup was as follows – the first signal intensity (SI) increment was observed in the right ventricle of the heart, followed by uptake in the left ventricle, reflecting the surge of systemic contrast spread. Immediately afterwards, between the 4th to 7th (24–42 s) acquisitions, the first SI uptake was noticed in the breast cancer region, while no SI uptake was noticed in the healthy surrounding lactating breast parenchyma. BPE was initially observed between the 5th and the 8th (30–48 s) acquisitions, in which the tumor was expressing continuous SI uptake. Until the 10th acquisition, both cancer and BPE exhibited a steady wash-in. Despite the variations and overlap between different patients, on the intra-subject basis, the cancer preceded the BPE in at least one acquisition, in all cases. A representative case of the ultrafast DCE of a PABC patient is provided in Fig. 1, highlighting the gradual SI kinetic distribution in cancer and BPE.

Overall, early visualization of breast malignancies by ultrafast DCE MRI of the breast, which was defined as a SI minimal increment of 30%, was apparent in all PABC patients ($n = 10$): 2/10 tumors were initially visible on the 4th acquisition (24 s), 5/10 on the 5th acquisition (30 s), 2/10 on the 6th acquisition (36 s) and 1/10 on the 7th acquisition (42 s). Three representative cases of ultrafast and conventional DCE images of lactating patients are provided in Fig. 2, demonstrating early visualization of breast cancer on ultrafast DCE with minimal BPE, as compared with the marked BPE in delayed acquisitions.

Tumor conspicuity with ultrafast and conventional DCE

CNR calculation on two ROIs, with normal and maximal BPE as references, revealed that the average tumor conspicuity on both analyses has gradually increased until reaching the highest values on the 6th ultrafast acquisition after approximately 36 s post-contrast ($CNR_{Normal} = 2.24 \pm 1.19$, and $CNR_{Max} = 1.64 \pm 1.19$). A diagram of the CNR analyses per acquisition is provided in Fig. 3. Overall, in 8/10 PABC

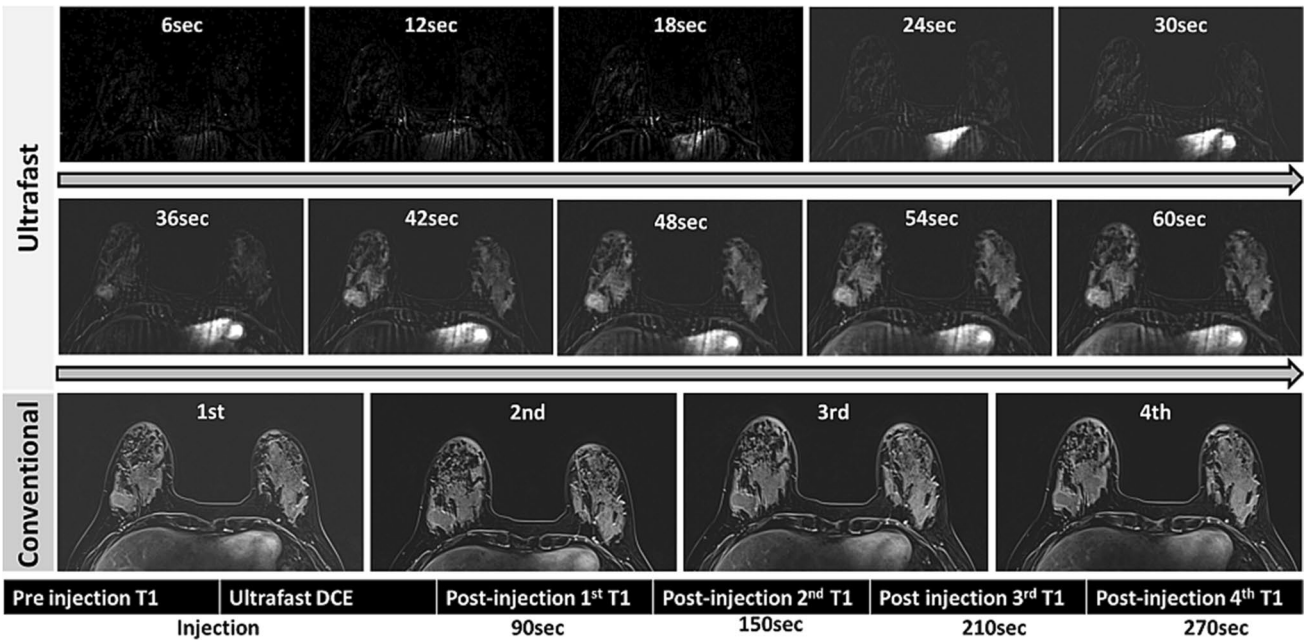

Fig. 1 Ultrafast and conventional DCE of PABC patient. Consecutive acquisitions of ultrafast ($n = 10$) and conventional ($n = 4$) DCE MRI of a representative lactating PABC patient are shown. On ultrafast, SI increase in the right and left of the heart, without breast enhancement are demonstrated in the first five acquisitions. In the sixth acquisition, contrast enhancement in the breast is solely identified in the breast cancer lesion (arrow) on the right breast, without surrounding BPE. Subsequently, on the 6th to 10th ultrafast acquisitions, a gradual increase in SI in both the tumor, as well as the surrounding lactating parenchyma is exhibited. Thereafter, on conventional DCE, marked BPE is demonstrated in both breasts, decreasing the conspicuity of the PABC lesion

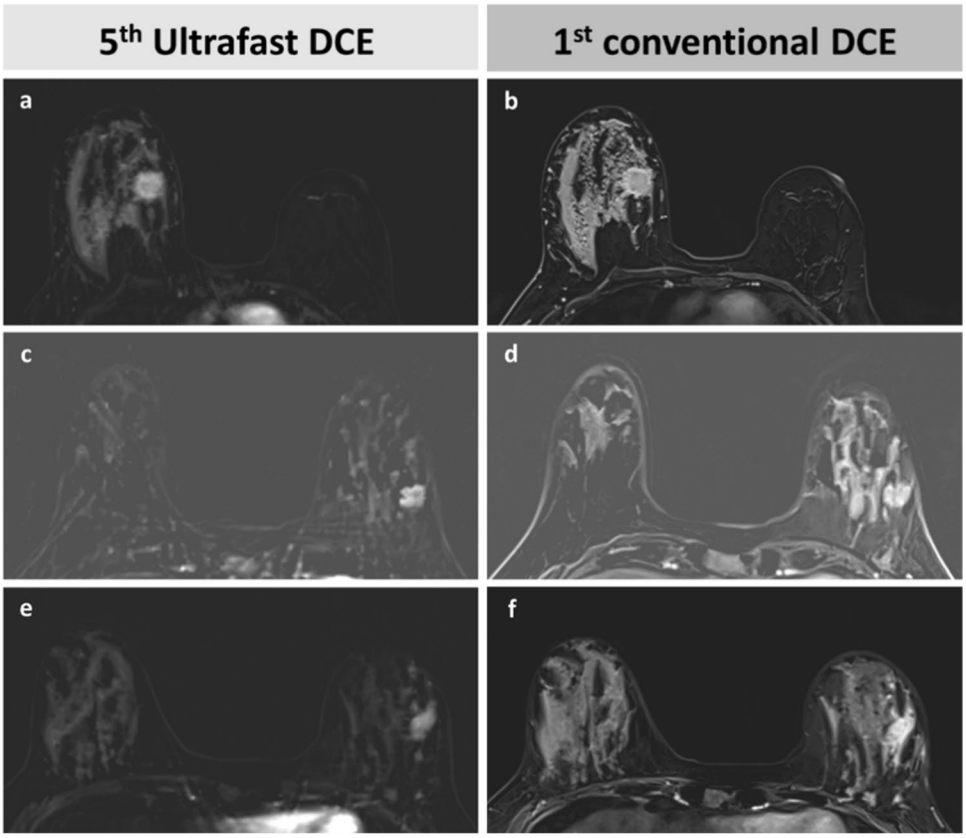

Fig. 2 Early visualization of PABC on ultrafast DCE. Subtracted DCE MR images of the 5th ultrafast acquisition (left-sided) and the respective 1st conventional acquisition (right-sided) of three representative lactating PABC patients are shown. On ultrafast, the PABC lesion is clearly visualized on the early acquisition (**a**, **c**, **e**), with mild (**a**) and minimal (**c**, **e**) surrounding BPE. On conventional DCE, however, the tumors are visualized on top of marked surrounding BPE (**b**, **d**, **f**), which reduces their conspicuity

cases, ultrafast acquisitions were able to provide superior tumor prominence as compared with the measurements on the conventional DCE images ($p < 0.05$).

Ultrafast kinetic parameters in tumor and BPE

A comparison of the three ultrafast-derived kinetic parameters, MS, TTE, and AUC, revealed significant differences between the tumor and the two BPE references, BPE_{Normal} and BPE_{Max}. Two representative cases with ultrafast parametric maps are given in Fig. 4 and Fig. 5, highlighting the parametric contrasts between the two types of enhancing processes. The complete ultrafast kinetic parameters are summarized in Table 2. Receiver operating characteristic curve analysis of the properties of the tumor and the healthy lactating parenchyma achieved the following results: For

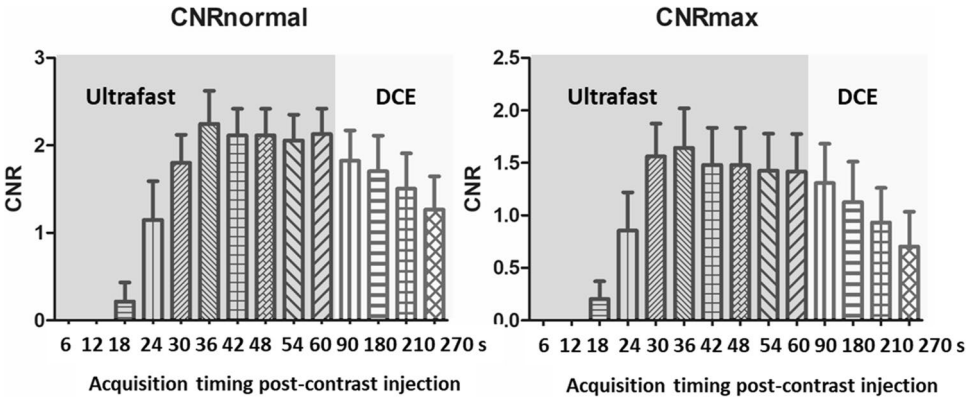

Fig. 3 CNR charts of ultrafast and conventional DCE**.** Column charts with average ± standard deviation of CNR measurements using ultrafast and conventional DCE are presented. Each column represents measurements in each of the time points of ultrafast and DCE acquisitions. CNRnormal and CNRmax were measured based on PABC datasets ($n = 10$) using the normal reciprocal contralateral BPE (left-sided) or the highest contralateral BPE (right-sided), respectively. On both CNRnormal and CNRmax measurements, the uppermost tumor conspicuity was attained on the 6th acquisition of ultrafast DCE

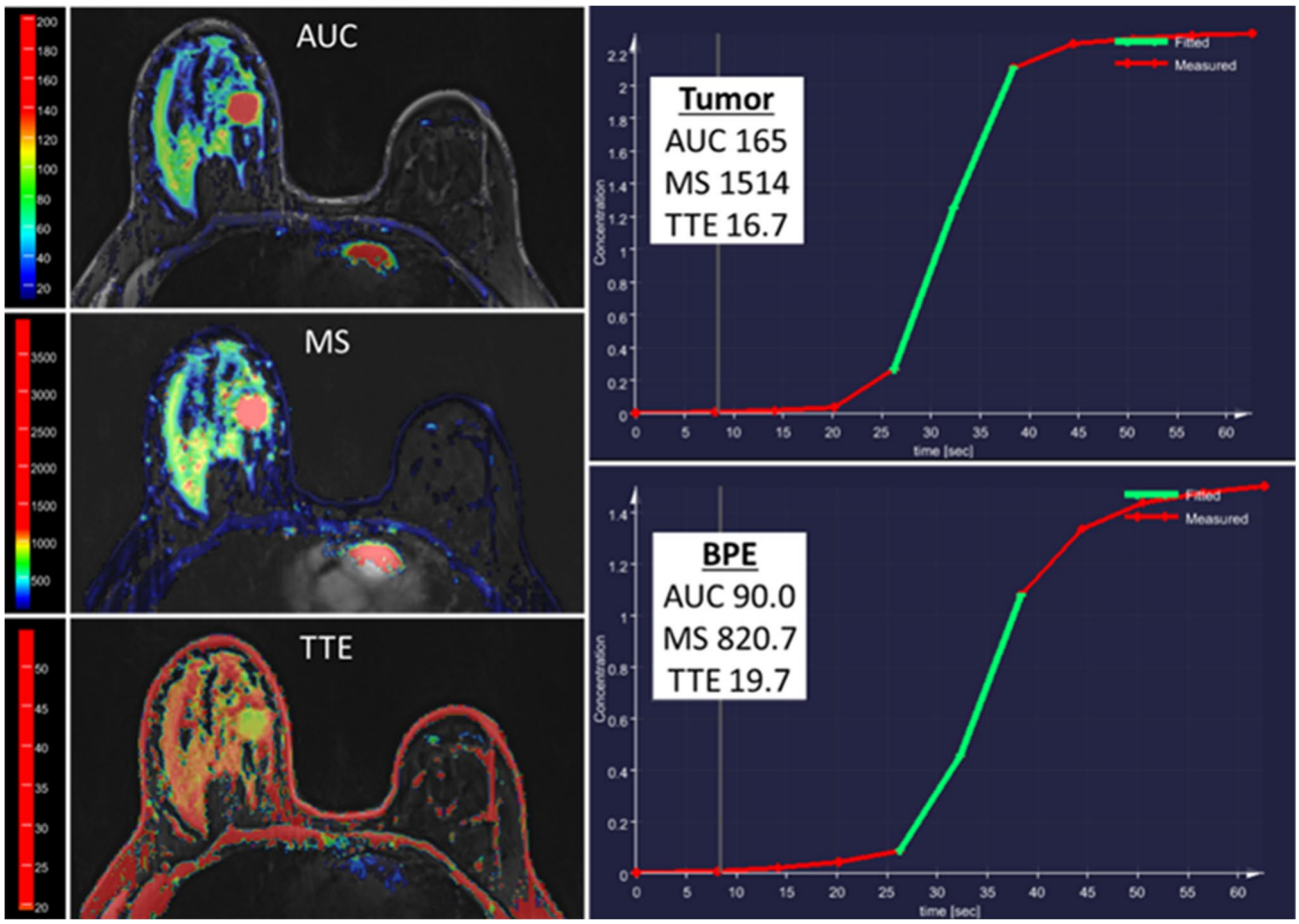

Fig. 4 Ultrafast parametric maps of lactating PABC patient. Parametric maps of a representative 36-year-old lactating PABC patient with a 2.0 cm grade 3 IDC are presented. All three ultrafast-derived maps of the parameters AUC, MS, and TTE exhibit excellent parametric contrast between the lesion and the surrounding BPE. Graphs of the enhancement kinetics of the tumor and BPE_{Normal} are also presented, exhibiting differences in the contrast enhancement of the slopes between the two entities

the AUC parameter, the obtained AUC was 0.86 ± 0.06 (95% confidence interval (CI) 0.74 to 0.98), with a threshold > 51.30 reaching a sensitivity of 80% and a specificity of 77.8%. For the MS parameter, the obtained AUC was 0.82 ± 0.07 (95% CI 0.69 to 0.95), with a threshold > 681.6 [units/s] reaching a sensitivity of 80% and a specificity of 74.4%. For the TTE parameter, the obtained AUC was 0.68 ± 0.08 (95% CI 0.52 to 0.83), with a threshold < 20.6 s reaching a sensitivity of 70% and a specificity of 64.4%.

BPE grades and ultrafast kinetic parameters in PABC patients vs. lactating controls

A comparison of the BPE grades for the lactating PABC patients and the healthy lactating controls showed a significant reduction among the former (2.87 ± 0.28 vs. 2.10 ± 0.84, $p < 0.005$). Moreover, significant differences in MS ($p < 0.05$) and TTE ($p < 0.005$) values were found among healthy controls and the cancer-free, contralateral breast of PABC patients based on measurements on the BPE_{Max} ROIs, whereas differences in AUC and ROI_{Normal} parameters did not reach statistical significance.

Discussion

In this study, we share our initial experience with the application of ultrafast DCE for breast MRI during lactation. In this setting, we encountered simultaneous intensely enhancing pathological and physiological processes (the tumor and the surrounding BPE) that affect the breast in PABC patients and create a diagnostic challenge for conventional DCE MRI. Yet, our preliminary results demonstrate how the high temporal resolution of the ultrafast sequence could be exploited to display improved contrast between the tumor and the lactation-associated BPE, based on differences in their enhancement kinetics.

Ultrafast DCE dedicated to breast imaging was originally published in 2014 by Mann et al using time-resolved

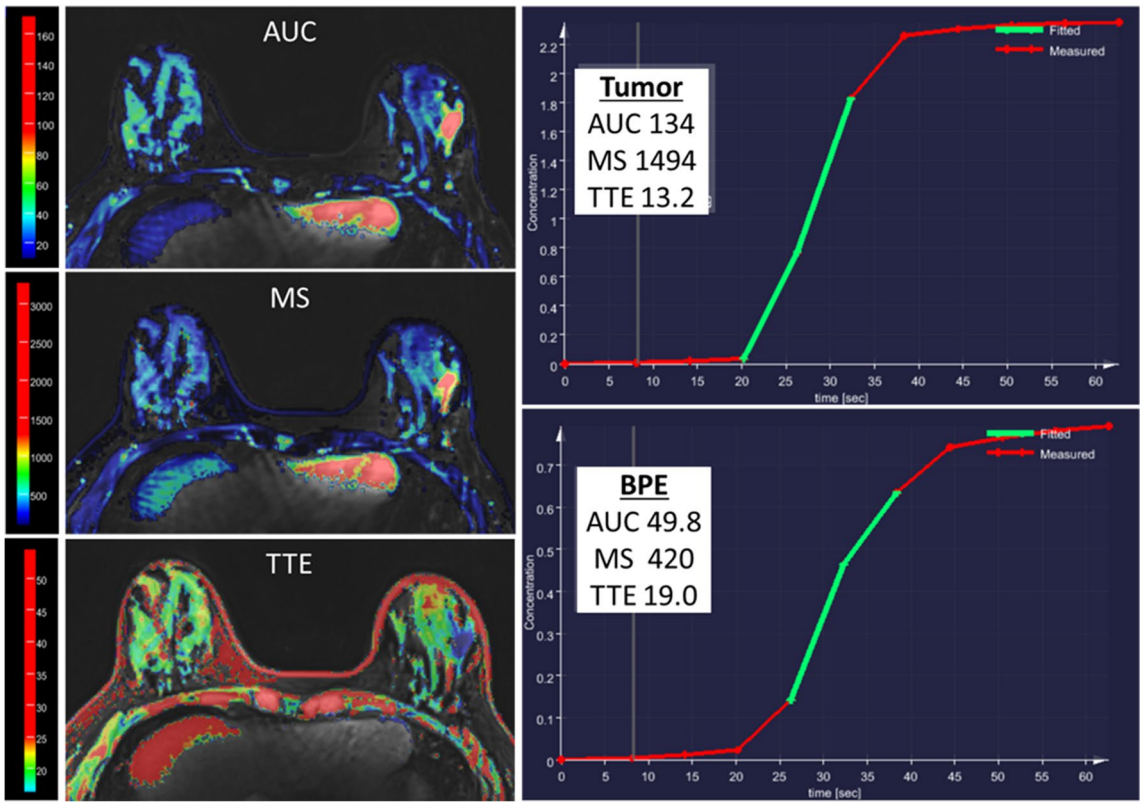

Fig. 5 Ultrafast parametric maps of lactating PABC patient. Parametric maps of 35 years old lactating PABC patients with multi-focal IDC are presented. All three ultrafast-derived maps of the parameters AUC, MS, and TTE exhibit excellent parametric contrast between the lesion and the surrounding BPE. Graphs of the enhancement kinetics of the tumor and BPE_{Normal} are also presented, exhibiting differences in the contrast enhancement slopes between the two entities

angiography with a stochastic trajectory (TWIST) sequence [17]. This technique relies on exploiting sparsely undersampled k-space in peripheral regions, while continuously sampling the k-space center to enable high temporal resolution with preserved spatial resolution [16]. The application of TWIST allowed the acquisition of rapid post-contrast T1-weighted images, with a temporal resolution of approximately 6 s [37]. Tracking and post-processing of the SI graph throughout the sequential ultrafast time points have led to the development of parametric maps that quantify wash-in properties. Initially, the MS parameter (percent per second), which represents the slope of the relative enhancement versus the time curve and reflects how rapidly a lesion enhances, provided discrimination between benign and malignant disease with high accuracy [17]. Later, the TTE parameter, measured from the time of aortic enhancement and reflects how early a lesion enhances, was derived and showed equivalent diagnostic ability [20, 27]. Finally, the

Table 2 Ultrafast DCE-derived kinetic parameters of tumor and BPE in PABC patients and healthy lactating controls

	PABC patients			Healthy lactating controls	
	Tumor	Contralateral BPE_{Normal}	Contralateral BPE_{Max}	BPE_{Normal}	BPE_{Max}
AUC	95.7 ± 47.2	22.4 ± 27.2***	36.4 ± 31.8***	26.0 ± 24.1	50.0 ± 22.8
MS (sec)	979.3 ± 416.4	325.8 ± 216.3**	444.8 ± 258.1**	397.6 ± 309.4	666.9 ± 284.5*
TTE (%/sec)	19.9 ± 4.0	31.4 ± 9.5*	27.9 ± 9.8*	24.9 ± 9.6	21.2 ± 4.2**

Mean ± SD ultrafast DCE-derived kinetic parameters of AUC, MS, and TTE of the tumor and BPE among PABC patients ($n = 10$) and healthy lactating patients ($n = 19$) are presented. Tumors parameters were intra-individually compared vs. the contralateral BPE parameters. A second comparison was between the BPE parameters of the PABC group vs. controls. Note: Significant differences were found in the three parameters between the tumor and the two contralateral BPE parameters. Interestingly, when comparing the BPE properties in the normal contralateral breast of the PABC cohort vs. the measurements in the healthy lactating controls, a significant reduction in MS and increase in TTE were found for the BPEmax in the PABC group, suggesting a possible vascular steal phenomenon in the former cohort. *$p < 0.05$, **$p < 0.01$, ***$p < 0.0005$

AUC parameter, defined as the initial area under the contrast enhancement vs. time curve [38], was also demonstrated to be useful in differentiating between benign and malignant breast lesions.

In this study, we utilized the unique advantages of ultrafast DCE MRI in order to manage the challenges posed by lactation-related BPE. For this purpose, we employed the GRASP ultrafast DCE-MRI technique, a comparable method to TWIST, which utilizes compressed sensing and parallel imaging to acquire simultaneous high spatial and temporal resolution with robustness to respiratory motion and flow [39, 40]. Previous investigations have reported an improvement in tumor conspicuity in breast cancer patients with moderate to marked BPE by using an ultrafast protocol [24, 38]. Indeed, our findings suggest that ultrafast acquisitions could differentiate these two enhancing entities, based on differences in their kinetic behavior. We also found inter-individual differences in the wash-in kinetics, and therefore there was not a single, crucial time point, but rather several periods in which the tumor visibility could be optimal. We noticed that PABC lesions begin to enhance one acquisition prior to the BPE. This short period permits a temporary window for lesion visualization, absent any interference from the BPE. Hence, this time point, in which the tumor is vividly enhancing and the BPE is only mild, is optimal for tumor visualization. Furthermore, ultrafast-derived parametric maps were found to be useful in distinguishing PABC lesions from BPE, including a comparison of regions in which the BPE was highest, BPE_{Max}. The most efficient discriminating parameter was AUC, followed by MS and TTE. Therefore, the implementation of these research tools in the routine reading sequences might be beneficial for radiologists to facilitate the interpretation of breast MRI of the lactating patient.

Interestingly, when comparing the BPE properties of the lactating breast cancer patients to the healthy lactating controls, significant differences were found. The BPE grade was closer to moderate among PABC patients, as compared with the almost exclusively marked BPE among the controls. As expected, significant differences were also found for the ultrafast-derived parameters of AUC and MS between the healthy lactating tissues in these two groups. This trend may minimize the interference of lactation-related BPE on tumor visibility in PABC patients. A possible explanation for this might be the "vascular steal phenomenon," in which the tumor's microenvironment "steals" the organ's normal vascular supply—a mechanism that has been described for several malignancies [41–43]. Similarly, a parallel observation has been reported in studies of 18-fluorine fluorodeoxyglucose (FDG), a glucose analogue uptake on positron-emitted tomography (PET). Reduced values have been measured in the contralateral, tumor-free breast tissue of patients with malignant breast tumors compared with that of patients with benign breast lesions [44]. Strikingly, reduced FDG uptake in both breasts among lactating breast cancer patients has been observed compared with lactating patients with active, non-breast malignancy. Similarly, this phenomenon has enabled the prompt visualization of PABC lesions in PET, on top of the diminished background parenchymal uptake (BPU) [45].

To date, ultrasound continues to serve as the first-line breast imaging modality in lactating patients [1], whereas the utility of mammography is relatively limited due to the high parenchymal density [7]. In pursuit of alternatives to DCE-MRI, unenhanced MRI, in the form of diffusion-weighted imaging (DWI) sequences [46], has been applied for the characterization of breast tissue in healthy lactating volunteers [47–51], as well as PABC patients [13, 52], showing promising results in detecting breast cancer among this challenging population. Nevertheless, reports from several research groups suggested that conventional DCE MRI might be useful during lactation [9–14]. Our results in the characterization of known PABC lesions propose that the application of ultrafast DCE may further facilitate the utilization of breast MRI during lactation for pretreatment assessment; however, it remains to be studied whether this technique would be beneficial in the setting of screening.

Several limitations of this study should be noted. Due to the infrequency of this population, the number of participants, and in particular, PABC patients, was small. Clearly, a greater sample size is required in order to specifically evaluate the diagnostic accuracy of ultrafast DCE among the lactating population, as well as to investigate for differences in enhancement kinetics arising from pathological markers, that may explain inter-individual variability we encountered. Furthermore, under-sampled radial acquisitions are prone to suboptimal image quality, in the form of 'streak' artifacts and reduced signal–noise-ratio [53]. This technique, as well as the parametric mapping software, are part of a work in progress and might benefit from technical developments in the near future [54].

In conclusion, ultrafast DCE MRI provided BPE-free visualization, improved tumor conspicuity, and quantitative, kinetic characterization of breast cancer in lactating patients. Continuous technical advances and clinical implementation of this method may enable radiologists to overcome BPE-related limitations of breast MRI and perform these scans during lactation.

Funding The authors state that this work has not received any funding.

Declarations

Guarantor The scientific guarantor of this publication is Dr. Noam Nissan.

Conflict of interest Three co-authors (Robert Grimm PhD, Nickel, Marcel Dominik PhD, Roccia, Elisa PhD) are employees of Siemens Healthcare, and they declared that they have no conflict of interest.

Statistics and biometry One of the authors has significant statistical expertise.

Informed consent Written informed consent was waived by the Institutional Review Board.

Ethical approval Institutional Review Board approval was obtained.

Methodology
- retrospective
- Case–control
- performed at one institution

References

1. Vashi R, Hooley R, Butler R et al (2013) Breast imaging of the pregnant and lactating patient: physiologic changes and common benign entities. AJR Am J Roentgenol 200(2):329–36
2. McManaman JL, Neville MC (2003) Mammary physiology and milk secretion. Adv Drug Deliv Rev 29;55(5):629–41
3. Geddes DT, Aljazaf KM, Kent JC et al (2012) Blood flow characteristics of the human lactating breast. J Hum Lact. https://doi.org/10.1177/0890334411435414
4. Nissan N, Bauer E, Efraim E et al (2022) Breast MRI during pregnancy and lactation : clinical challenges and technical advances. Insights Imaging. https://doi.org/10.1186/s13244-022-01214-7
5. Amant F, Von Minckwitz G, Han SN et al (2013) Prognosis of women with primary breast cancer diagnosed during pregnancy: results from an international collaborative study. J Clin Oncol. https://doi.org/10.1200/JCO.2012.45.6335
6. Carmichael H, Matsen C, Freer P et al (2017) Breast cancer screening of pregnant and breastfeeding women with BRCA mutations. Breast Cancer Res Treat 162(2):225–230
7. diFlorio-Alexander RM, Slanetz PJ, Moy L et al (2018) ACR appropriateness Criteria® breast imaging of pregnant and lactating women. J Am Coll Radiol. https://doi.org/10.1016/j.jacr.2018.09.013
8. Kieturakis AJ, Wahab RA, Vijapura C, Mahoney MC (2021) Current recommendations for breast imaging of the pregnant and lactating patient. AJR Am J Roentgenol 6(6):1462–1475
9. Oh SW, Lim HS, Moon SM et al (2017) MR imaging characteristics of breast cancer diagnosed during lactation. Br J Radiol. https://doi.org/10.1259/bjr.20170203
10. Espinosa LA, Daniel BL, Vidarsson L et al (2005) The lactating breast: contrast-enhanced MR imaging of normal tissue and cancer. Radiology. https://doi.org/10.1148/radiol.2372040837
11. Taron J, Fleischer S, Preibsch H et al (2019) Background parenchymal enhancement in pregnancy-associated breast cancer: a hindrance to diagnosis? Eur Radiol. https://doi.org/10.1007/s00330-018-5721-7
12. Myers KS, Green LA, Lebron L, Morris EA (2017) Imaging appearance and clinical impact of preoperative breast MRI in pregnancy-associated breast cancer. AJR Am J Roentgenol. https://doi.org/10.2214/AJR.16.17124
13. Nissan N, Allweis T, Menes T et al (2020) Breast MRI during lactation: effects on tumor conspicuity using dynamic contrast-enhanced (DCE) in comparison with diffusion tensor imaging (DTI) parametric maps. Eur Radiol. https://doi.org/10.1007/s00330-019-06435-x
14. Nissan N, Massasa EEM, Bauer E et al (2022) MRI can accurately diagnose breast cancer during lactation. Eur Radiol. https://doi.org/10.1007/s00330-022-09234-z
15. Nissan N, Sorin V, Bauer E et al (2021) MRI of the lactating breast : computer-aided diagnosis false positive rates and background parenchymal enhancement kinetic features. Acad Radiol 1–10. https://doi.org/10.1016/j.acra.2021.11.003
16. Lustig M, Donoho D, Pauly JM (2007) Sparse MRI: The application of compressed sensing for rapid MR imaging. Magn Reson Med. https://doi.org/10.1002/mrm.21391
17. Mann RM, Mus RD, Van Zelst J et al (2014) A novel approach to contrast-enhanced breast magnetic resonance imaging for screening: high-resolution ultrafast dynamic imaging. Invest Radiol. https://doi.org/10.1097/RLI.0000000000000057
18. Platel B, Mus R, Welte T et al (2014) Automated characterization of breast lesions imaged with an ultrafast DCE-MR protocol. IEEE Trans Med Imaging. https://doi.org/10.1109/TMI.2013.2281984
19. Goto M, Sakai K, Yokota H et al (2019) Diagnostic performance of initial enhancement analysis using ultra-fast dynamic contrast-enhanced MRI for breast lesions. Eur Radiol 29:1164–1174. https://doi.org/10.1007/s00330-018-5643-4
20. Honda M, Kataoka M, Onishi N et al (2020) New parameters of ultrafast dynamic contrast-enhanced breast MRI using compressed sensing. J Magn Reson Imaging. https://doi.org/10.1002/jmri.26838
21. Shin SU, Cho N, Kim SY et al (2020) Time-to-enhancement at ultrafast breast DCE-MRI: potential imaging biomarker of tumour aggressiveness. Eur Radiol. https://doi.org/10.1007/s00330-020-06693-0
22. Vreemann S, Rodriguez-Ruiz A, Nickel D et al (2017) Compressed sensing for breast MRI: resolving the trade-off between spatial and temporal resolution. Invest Radiol. https://doi.org/10.1097/RLI.0000000000000384
23. Yamaguchi K, Nakazono T, Egashira R et al (2021) Maximum slope of ultrafast dynamic contrast-enhanced MRI of the breast: comparisons with prognostic factors of breast cancer. Jpn J Radiol. https://doi.org/10.1007/s11604-020-01049-6
24. Kim SY, Cho N, Hoi Y et al (2020) Ultrafast dynamic contrast-enhanced breast MRI: Lesion conspicuity and size assessment according to background parenchymal enhancement. Korean J Radiol. https://doi.org/10.3348/kjr.2019.0567
25. Kim JH, Park VY, Shin HJ et al (2022) Ultrafast dynamic contrast-enhanced breast MRI: association with pathologic complete response in neoadjuvant treatment of breast cancer. Eur Radiol. https://doi.org/10.1007/s00330-021-08530-4
26. Kim JJ, Kim JY, Hwangbo L et al (2021) Ultrafast dynamic contrast-enhanced MRI using compressed sensing: associations of early kinetic parameters with prognostic factors of breast cancer. AJR Am J Roentgenol 217:56–63. https://doi.org/10.2214/AJR.20.23457
27. Mus RD, Borelli C, Bult P et al (2017) Time to enhancement derived from ultrafast breast MRI as a novel parameter to discriminate benign from malignant breast lesions. Eur J Radiol 89:90–96. https://doi.org/10.1016/j.ejrad.2017.01.020
28. Oldrini G, Fedida B, Poujol J et al (2017) Abbreviated breast magnetic resonance protocol: value of high-resolution temporal dynamic sequence to improve lesion characterization. Eur J Radiol. https://doi.org/10.1016/j.ejrad.2017.07.025
29. Onishi N, Sadinski M, Gibbs P et al (2020) Differentiation between subcentimeter carcinomas and benign lesions using kinetic parameters derived from ultrafast dynamic contrast-enhanced breast MRI. Eur Radiol. https://doi.org/10.1007/s00330-019-06392-5
30. Pelissier M, Ambarki K, Salleron J, Henrot P (2021) Maximum slope using ultrafast breast DCE-MRI at 1.5 Tesla: a potential tool

for predicting breast lesion aggressiveness. Eur Radiol. https://doi.org/10.1007/s00330-021-08089-0
31. Peter SC, Wenkel E, Weiland E et al (2020) Combination of an ultrafast TWIST-VIBE Dixon sequence protocol and diffusion-weighted imaging into an accurate easily applicable classification tool for masses in breast MRI. Eur Radiol. https://doi.org/10.1007/s00330-019-06608-8
32. Bauer E, Levy MS, Domachevsky L et al (2021) Background parenchymal enhancement and uptake as breast cancer imaging biomarkers: a state-of-the-art review. Clin Imaging 83:41–50. https://doi.org/10.1016/j.clinimag.2021.11.021
33. Yoon JH, Lee JM, Yu MH et al (2022) Simultaneous evaluation of perfusion and morphology using GRASP MRI in hepatic fibrosis. Eur Radiol. https://doi.org/10.1007/s00330-021-08087-2
34. Tomppert A, Wuest W, Wiesmueller M et al (2021) Achieving high spatial and temporal resolution with perfusion MRI in the head and neck region using golden-angle radial sampling. Eur Radiol. https://doi.org/10.1007/s00330-020-07263-0
35. Song SE, Seo BK, Cho KR et al (2020) Preoperative tumor size measurement in breast cancer patients: which threshold is appropriate on computer-aided detection for breast MRI? Cancer Imaging. https://doi.org/10.1186/s40644-020-00307-0
36. Furman-Haran E, Grobgeld D, Nissan N et al (2016) Can diffusion tensor anisotropy indices assist in breast cancer detection? J Magn Reson Imaging. https://doi.org/10.1002/jmri.25292
37. Gao Y, Heller SL (2020) Abbreviated and ultrafast breast MRI in clinical practice. Radiographics 40:1507–1527. https://doi.org/10.1148/rg.2020200006
38. Pineda FD, Medved M, Wang S et al (2016) Ultrafast bilateral DCE-MRI of the breast with conventional Fourier sampling: preliminary evaluation of semi-quantitative analysis. Acad Radiol. https://doi.org/10.1016/j.acra.2016.04.008
39. Kim SG, Feng L, Grimm R et al (2016) Influence of temporal regularization and radial undersampling factor on compressed sensing reconstruction in dynamic contrast enhanced MRI of the breast. J Magn Reson Imaging. https://doi.org/10.1002/jmri.24961
40. Heacock L, Gao Y, Heller SL et al (2017) Comparison of conventional DCE-MRI and a novel golden-angle radial multicoil compressed sensing method for the evaluation of breast lesion conspicuity. J Magn Reson Imaging. https://doi.org/10.1002/jmri.25530
41. Bailey KM, Cornnell HH, Ibrahim-Hashim A et al (2014) Evaluation of the "steal" phenomenon on the efficacy of hypoxia activated prodrug th-302 in pancreatic cancer. PLoS One. https://doi.org/10.1371/journal.pone.0113586
42. Forster J, Harriss-Phillips W, Douglass M, Bezak E (2017) A review of the development of tumor vasculature and its effects on the tumor microenvironment. Hypoxia. https://doi.org/10.2147/hp.s133231
43. Hughes P, Miranda R, Doyle AJ (2019) MRI imaging of soft tissue tumours of the foot and ankle. Insights Imaging 10:60
44. Leithner D, Helbich TH, Bernard-Davila B et al (2020) Multiparametric 18F-FDG PET/MRI of the breast: are there differences in imaging biomarkers of contralateral healthy tissue between patients with and without breast cancer? J Nucl Med. https://doi.org/10.2967/jnumed.119.230003
45. Nissan N, Sandler I, Eifer M et al (2020) Physiologic and hypermetabolic breast 18-F FDG uptake on PET/CT during lactation. Eur Radiol. https://doi.org/10.1007/s00330-020-07081-4
46. Partridge SC, Nissan N, Rahbar H et al (2017) Diffusion-weighted breast MRI: clinical applications and emerging techniques. J Magn Reson Imaging 45(2):337–355
47. Iima M, Kataoka M, Sakaguchi R et al (2018) Intravoxel incoherent motion (IVIM) and non-Gaussian diffusion MRI of the lactating breast. Eur J Radiol Open 5:24–30. https://doi.org/10.1016/j.ejro.2018.01.003
48. Nissan N, Furman-Haran E, Shapiro-Feinberg M et al (2014) Diffusion-tensor MR imaging of the breast: hormonal regulation. Radiology 271:672–680. https://doi.org/10.1148/radiol.14132084
49. Nissan N, Furman-Haran E, Feinberg-Shapiro M et al (2014) Tracking the mammary architectural features and detecting breast cancer with magnetic resonance diffusion tensor imaging. J Vis Exp 1–18. https://doi.org/10.3791/52048
50. Nissan N, Furman-Haran E, Shapiro-Feinberg M et al (2017) Monitoring In-vivo the mammary gland microstructure during morphogenesis from lactation to post-weaning using diffusion tensor MRI. J Mammary Gland Biol Neoplasia. https://doi.org/10.1007/s10911-017-9383-x
51. Sah RG, Agarwal K, Sharma U et al (2015) Characterization of malignant breast tissue of breast cancer patients and the normal breast tissue of healthy lactating women volunteers using diffusion MRI and in vivo 1H MR spectroscopy. J Magn Reson Imaging 41:169–174. https://doi.org/10.1002/jmri.24507
52. Nissan N, Furman-Haran E, Allweis T et al (2018) Noncontrast breast MRI during pregnancy using diffusion tensor imaging: a feasibility study. J Magn Reson Imaging 1–10. https://doi.org/10.1002/jmri.26228
53. Sagawa H, Kataoka M, Kanao S et al (2019) Impact of the number of iterations in compressed sensing reconstruction on ultrafast dynamic contrast-enhanced breast mr imaging. Magn Reson Med Sci. https://doi.org/10.2463/mrms.mp.2018-0015
54. Feng L (2022) Golden-angle radial MRI: basics, advances, and applications. J Magn Reson Imaging 56:45–62. https://doi.org/10.1002/jmri.28187